BioMedical Engineering OnLine

RESEARCH

Open Access

A transcriptomic analysis of dental pulp stem cell senescence in vitro

Jidong Xu[1], Mingchang Hu[1], Longfei Liu[2], Xuecheng Xu[1], Linlin Xu[1] and Yu Song[3*]

*Correspondence:
bmusy2002sy@163.com

[1] School of Stomatology, Qingdao University, Qingdao 266003, China
[2] Qingdao Engineering Vocational College, Qingdao 266000, China
[3] Department of Orthodontics, Qingdao Stomatological Hospital Affiliated to Qingdao University, Qingdao 266001, China

Abstract

Background/purpose: The use of human dental pulp stem cells (hDPSCs) as autologous stem cells for tissue repair and regenerative techniques is a significant area of global research. The objective of this study was to investigate the effects of long-term in vitro culture on the multidifferentiation potential of hDPSCs and the potential molecular mechanisms involved.

Materials and methods: The tissue block method was used to extract hDPSCs from orthodontic-minus-extraction patients, which were then expanded and cultured in vitro for 12 generations. Stem cells from passages three, six, nine, and twelve were selected. Flow cytometry was used to detect the expression of stem cell surface markers, and CCK-8 was used to assess cell proliferation. β-Galactosidase staining was employed to detect cellular senescence, Alizarin Red S staining to assess osteogenic potential, and Oil Red O staining to evaluate lipogenic capacity. RNA sequencing (RNA-seq) was conducted to identify differentially expressed genes in DPSCs and investigate their potential mechanisms.

Results: With increasing passage numbers, pulp stem cells showed an increase in senescence and a decrease in proliferative capacity and osteogenic–lipogenic multidifferentiation potential. The expression of stem cell surface markers CD34 and CD45 was stable, whereas the expression of CD73, CD90, and CD105 decreased with increasing passages. According to the RNA-seq analysis, the differentially expressed genes CFH, WNT16, HSD17B2, IDI1, and COL5A3 may be associated with stem cell senescence.

Conclusion: Increased in vitro expansion induced cellular senescence in pulp stem cells, which resulted in a reduction in their proliferative capacity and osteogenic–lipogenic differentiation potential. The differential expression of genes such as CFH, WNT16, HSD17B2, IDI1, and COL5A3 may represent a potential mechanism for the induction of cellular senescence in pulp stem cells.

Keywords: Dental pulp stem cells, Senescence, Multiple differentiation potential, Transcriptome sequencing

Introduction

Integrity of the alveolar bone is a prerequisite for successful dental treatment. However, bone defects caused by periodontal disease, trauma, tumours, and inappropriate orthodontic manipulation have always plagued clinicians. Currently, traditional bone repair

techniques such as autologous bone grafting or bone graft substitutes have not achieved satisfactory repair results [1]. In recent years, tissue-engineered bone repair and regeneration techniques based on autologous stem cells have attracted considerable interest worldwide. Obtaining autologous seed stem cells with good activity and functionality is the key to research.

Mesenchymal stem cells (MSCs) are pluripotent cells with a fibroblast-like morphology that originate from the mesoderm and can be induced to differentiate into osteoblasts, chondrocytes, and adipocytes under appropriate conditions [2]. Stem cell therapy is the process of implanting autologous or allogeneic stem cells into the human body after in vitro manipulation, such as isolation, identification, purification, expansion, and induction of differentiation. However, the number of stem cells required for each application in research and clinics is considerable, even with bone marrow, which is rich in stem cells, being unable to meet the demand. Consequently, to rapidly obtain a large number of MSCs for research or clinical applications, increasing the number of cells through in vitro cell expansion and culture is unavoidable [3].

Dental pulp stem cells (DPSCs) are undifferentiated MSCs extracted from the dental pulp tissue [3]. They are considered the most accessible and promising multifunctional MSCs for tissue engineering and regenerative medicine because of their ease of accessibility, expansion, and preservation, high activity, and low tumourigenicity compared with other MSCs in the human body [4–9]. However, storage of DPSCs in the human body is limited, making it difficult to meet the requirements of tissue engineering and regenerative medicine. In vitro amplification is necessary to obtain a sufficient number of DPSCs for therapeutic use [10]. It is important to note that in the standard culture state, due to the limited number of divisions, stem cells divide into a certain number of generations before entering a proliferative arrest, i.e., cellular senescence [11]. This process leads to a functional decline of stem cells, stagnant cell growth, significantly weakened differentiation ability, and an increased number of apoptotic cells, which are no longer suitable for tissue engineering therapy and limit their clinical application [11, 12]. Consequently, the quality control of stem cells prior to their application in tissue engineering must include an in vitro passaging process.

Cellular senescence is strongly regulated at the post-transcriptional level, with the interaction of RNA-binding proteins and non-coding RNAs with senescence-associated messenger RNAs (mRNAs) playing a pivotal role in this regulation [13]. It has been demonstrated that cellular senescence is affected by specific chemical modifications of mRNAs [13]. The current research on mRNA modifications has focused on the role of mRNA methylation, with studies investigating its potential involvement in cancer, obesity, and other age-related pathologies [14, 15]. Indeed, there is accumulating evidence that mRNA modification may be closely related to cellular senescence.

The molecular mechanism of cellular senescence resulting from the long-term in vitro culture of DPSCs remains unknown, and there are currently no cell culture protocols that can delay or prevent the senescence of DPSCs. The objective of this study was to investigate the effects of long-term in vitro expansion culture on the morphology, immunophenotype, proliferation, and osteogenic–lipogenic multidifferentiation potential of DPSCs, as well as the changes in mRNA expression of DPSCs during long-term in vitro expansion culture. Furthermore, we aimed to identify the potential molecular

mechanisms that trigger DPSC senescence. The regulation of DPSC senescence plays a pivotal role in the clinical application of stem cells. Therefore, an in-depth understanding of DPSC senescence mechanisms is crucial for developing strategies that promote the regenerative potential of DPSCs to maintain tissue function.

Results

Characterisation of DPSCs at different passages

Within 10 days of primary culture (P0), spindle-shaped cells arranged in a whirlpool shape were observed around the dental pulp tissue. The cells were expanded to 12 generations in subsequent in vitro passaged cultures. As the number of in vitro passages increased, cell morphology exhibited distinguishable replicative senescence changes. The cells enlarged and acquired irregular and flattened shapes, while the nuclei became thinner. The cytoplasm was granular and contained elevated levels of cellular debris and inclusions (Fig. 1A). A few cells proliferated without adhering to the walls. Flow cytometry analysis revealed that DPSCs at P3 expressed CD73, CD90, and CD105 at high levels and CD34 and CD45 at low levels, thereby verifying the immunophenotype of DPSCs (Fig. 1B). As the number of passages increased, the percentages of DPSCs expressing CD34 and CD45 remained stable. However, the percentage of DPSCs expressing CD73, CD90, and CD105 decreased. This change was particularly significant in DPSCs cultured up to P12 (Fig. 1B, Table 1). These findings imply that surface marker expression levels were altered to some extent during continuous in vitro cultivation.

Changes in senescence and proliferation of DPSCs at different passages

DPSCs were cultured for 5 days, and changes in their proliferative capacity were measured using the CCK-8 method. The results demonstrated that the third generation had the fastest proliferation rate, with subsequent generations exhibiting progressively slower proliferation rates (Fig. 2A). This study revealed a decline in the proliferative potential of DPSCs with an increasing number of passages during prolonged in vitro culture. SA-β-gal staining was conducted on the third, sixth, ninth, and twelfth generations of DPSCs to examine senescence at varying passage numbers. Under microscopic inspection, cells with dark blue staining in their cytoplasm were considered SA-β-gal positive, indicating senescent cells. A minor proportion of blue cells was detected in the third-generational DPSCs (Fig. 2B), which yielded an SA-β-gal positivity rate of 7%. The rate of SA-β-gal positivity was recorded as $10.08 \pm 1.08\%$, $17.5 \pm 1.45\%$ and $27 \pm 2.89\%$ at P6, P9, and P12, respectively. In addition, the number of cells displaying dark blue staining gradually increased with increasing in vitro expansion ($P < 0.05$) (Fig. 2B). This observation indicates a gradual increase in the proportion of SA-β-gal positive cells during succeeding passages of DPSCs in vitro (Fig. 2C); cells undergo a senescent phenotype due to multiple in vitro expansions.

Changes in the multidifferentiation potential of DPSCs with different numbers of passages

Osteogenic and lipogenic differentiation experiments involved inducing lipogenic and osteogenic differentiation for 14 and 21 days, respectively. The results obtained from Alizarin Red S (ARS) and Oil Red O (ORO) staining showed that cells from P3 and P6 generations had good osteogenic and lipogenic characteristics. Mineralised nodules and

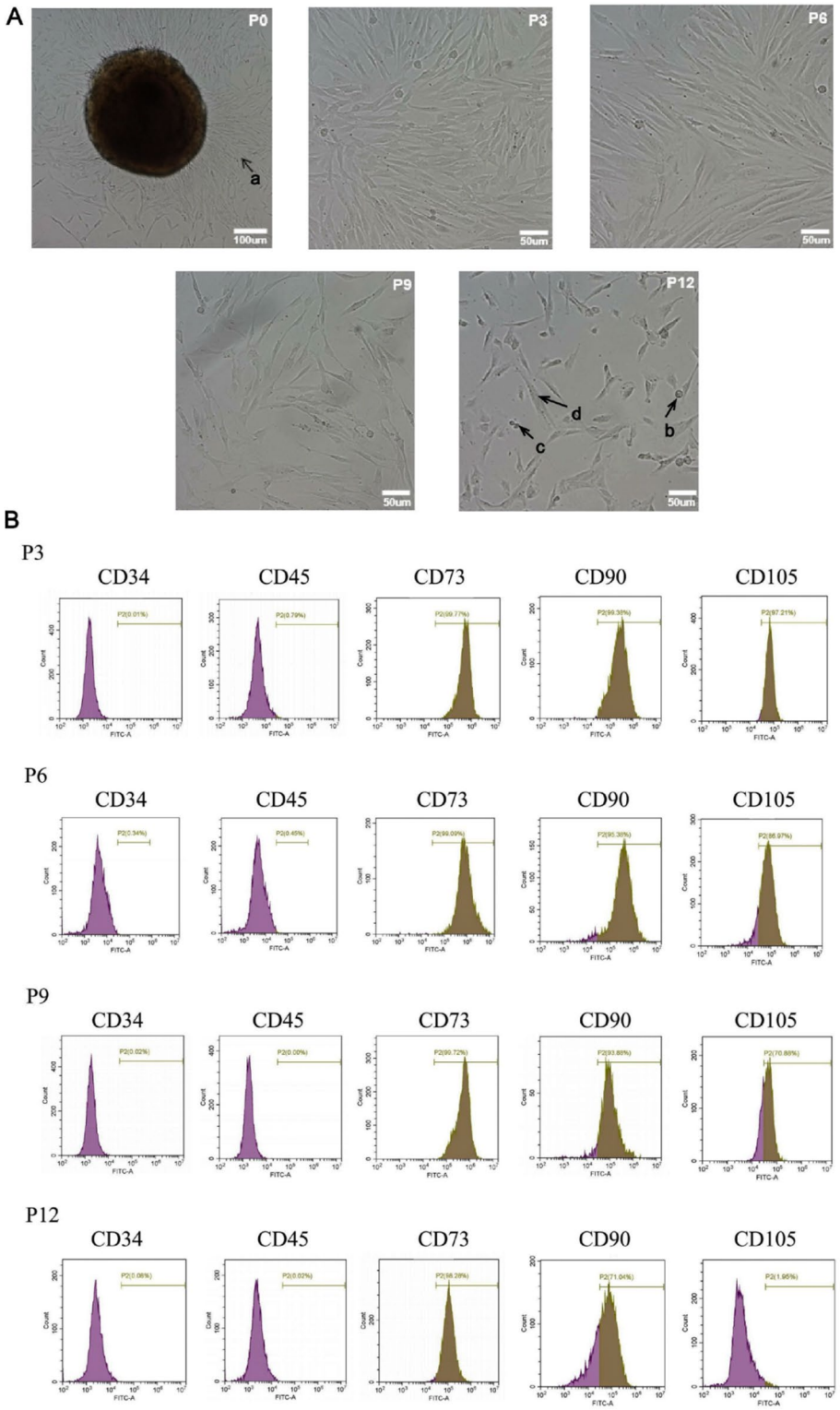

Fig. 1 Morphological and immunophenotypic changes in primary and passaged DPSCs. **A** Morphology of primary cells (P0) and passaged cells (P3, P6, P9, and P12); a: primary cells; b: nucleus; c: cellular debris and inclusions; d: cytoplasm. **B** The expression of surface markers in passaged cells (P3, P6, P9, and P12)

Table 1 Quantitative analysis of surface markers expression in DPSCs at P3, P6, P9, and P12 (n = 20, mean ± SD)

Marker	P3	P6	P9	P12	F	P
CD34	1.86 ± 2.34	0.67 ± 0.53	3.96 ± 6.47	0.21 ± 0.14	0.9729	0.4375
CD45	2.51 ± 3.79	0.56 ± 0.78	4.89 ± 8.45	0.39 ± 0.76	0.8153	0.5098
CD73	99.30 ± 0.32	96.97 ± 4.84	99.50 ± 0.23	46.26 ± 53.12	3.858	0.0382
CD90	98.96 ± 0.39	96.88 ± 1.48	91.10 ± 11.46	29.38 ± 32.30^{abc}	15.08	0.0002
CD105	91.29 ± 4.25	84.93 ± 4.87	71.60 ± 4.36^{ab}	1.14 ± 1.02^{abc}	446.0	< 0.0001

There were no significant differences in the expression of CD34 and CD45 in DPSCs at different passages ($P > 0.05$); the expression of CD73, CD90, and CD105 showed a decreasing trend with the increasing passage times ($P < 0.05$). $^{a}P < 0.01$ vs. P3; $^{b}P < 0.01$ vs. P6; $^{c}P < 0.01$ vs. P9 (n = 20)

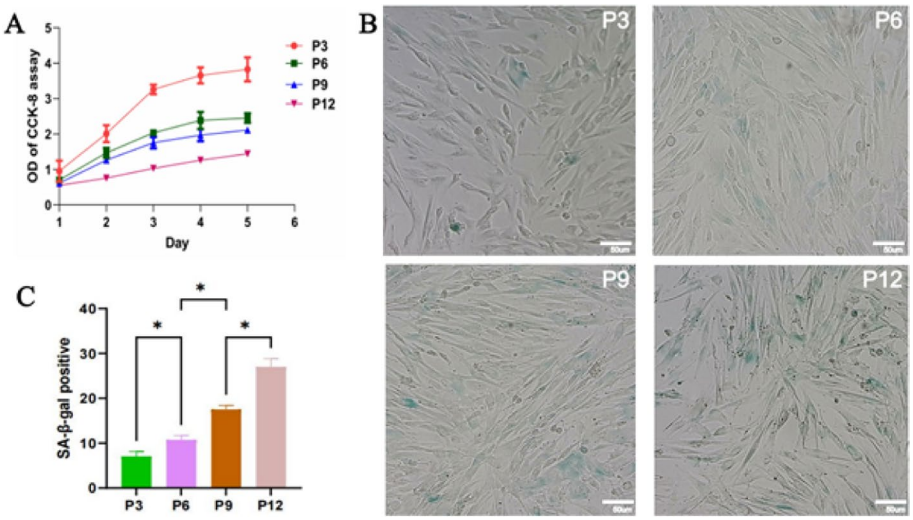

Fig. 2 The proliferation and senescence of DPSCs at P3, P6, P9, and P12. **A** The proliferation ability of DPSCs at different passage times was detected by CCK-8. **B**, **C** β-Galactosidase staining and the percentage of positive stained DPSCs at different passages. *$P < 0.05$ (n = 20)

lipid droplets were observed under a microscope. Stem cells that underwent numerous passages, specifically P9 and P12, displayed a decreased potential for osteogenic and lipogenic differentiation. Additionally, a higher number of apoptotic cells were observed, and there was a shift in cell morphology from an initial long spindle to an oval-like shape. Retention of the mineralised nodules and lipid droplets was challenging as passage number increased (Fig. 3A, B). Quantitative analyses indicated that the osteogenic and lipogenic abilities of DPSCs decreased as the number of in vitro passages increased (Fig. 3C, D). These results suggested that continuous passaging in vitro induces senescence in DPSCs. As the number of in vitro passages increased, the heterogeneity of cell morphology increased, the proliferative capacity and multidifferentiation potential decreased, and the proportion of SA-β-gal positive cells increased.

Differential gene expression profiles of DPSCs during aging in vitro

Sixteen samples from 4 groups of DPSCs at P3, P6, P9, and P12 were subjected to mRNA sequencing (mRNA-seq). This sequencing detected 33,638 expressed genes and differentially expressed (DE) mRNAs were screened using the $|\log2FC| \geq 1$ and P-value < 0.05

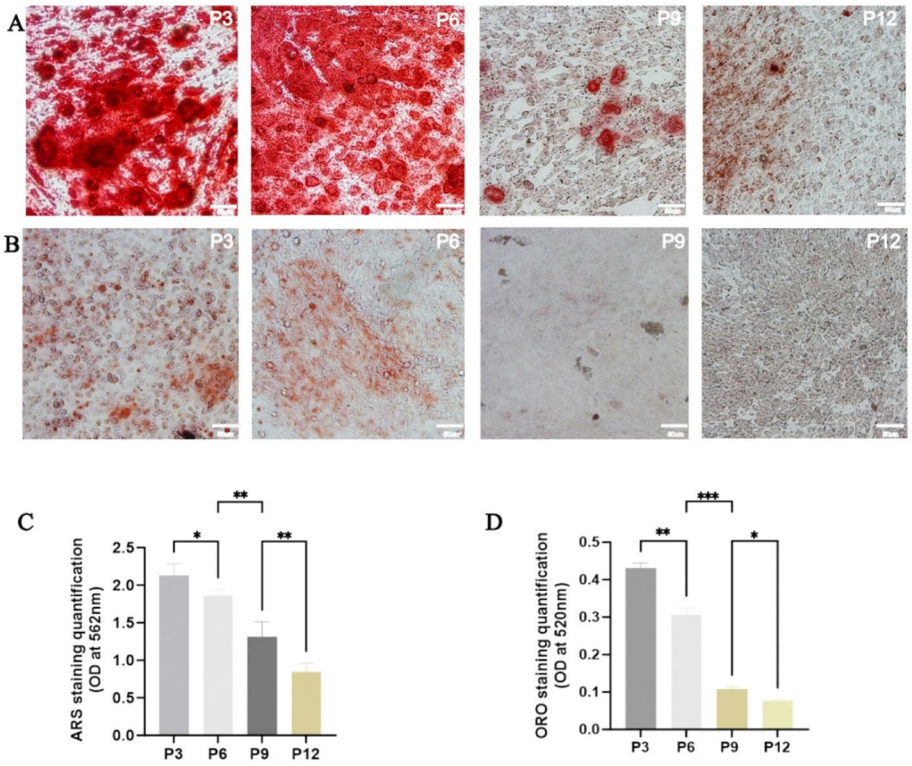

Fig. 3 The multidifferentiation capacity of DPSCs at P3, P6, P9, and P12 generation. **A** ARS staining for osteogenic differentiation. **B** ORO staining for lipogenic differentiation. **C**, **D** Quantitative analysis of ARS and ORO staining. *$P < 0.05$, **$P < 0.01$, ***$P < 0.001$ (n = 20)

criteria. Compared with P3, there were 283 DE mRNAs in P6, of which 98 were up-regulated and 185 down-regulated (Fig. 4A), 536 DE mRNAs in P9, of which 347 were up-regulated and 189 down-regulated (Fig. 4B), and 1159 DE mRNAs in P12, of which 692 were up-regulated and 467 down-regulated (Fig. 4C). DE mRNAs were depicted using heat polygraph (Fig. 4D), in which the most significant changes in DE mRNAs were observed in P12. Table 2 shows the top 10 mRNAs with the largest up-regulation or down-regulation in P12 compared with P3, including CFH, WNT16, and IDI1. These differentially altered RNAs were closely associated with the signalling pathways that regulate stem cell pluripotency.

mRNA GO and KEGG analysis

The sequencing results showed the most pronounced differential changes in P12 and P3. We performed Gene Ontology (GO) and Kyoto Encyclopedia of Genes and Genomes (KEGG) analyses of P12 and P3 DE mRNA. The top 20 GO terms related to biological processes, cellular components, and molecular functions are shown in Fig. 5A–C. The top 10 GO terms related to bioprocesses and the associated DE mRNA information are shown in Table 3 ($P < 0.05$). These bioprocess-related mRNAs were closely related to the regulation of stress response, cell proliferation, cellular bioprocess regulation, and organ development. KEGG analysis of DE mRNA revealed that 35 pathways were significantly altered ($P < 0.05$) in DPSCs during in vitro senescence. The top 20 most enriched

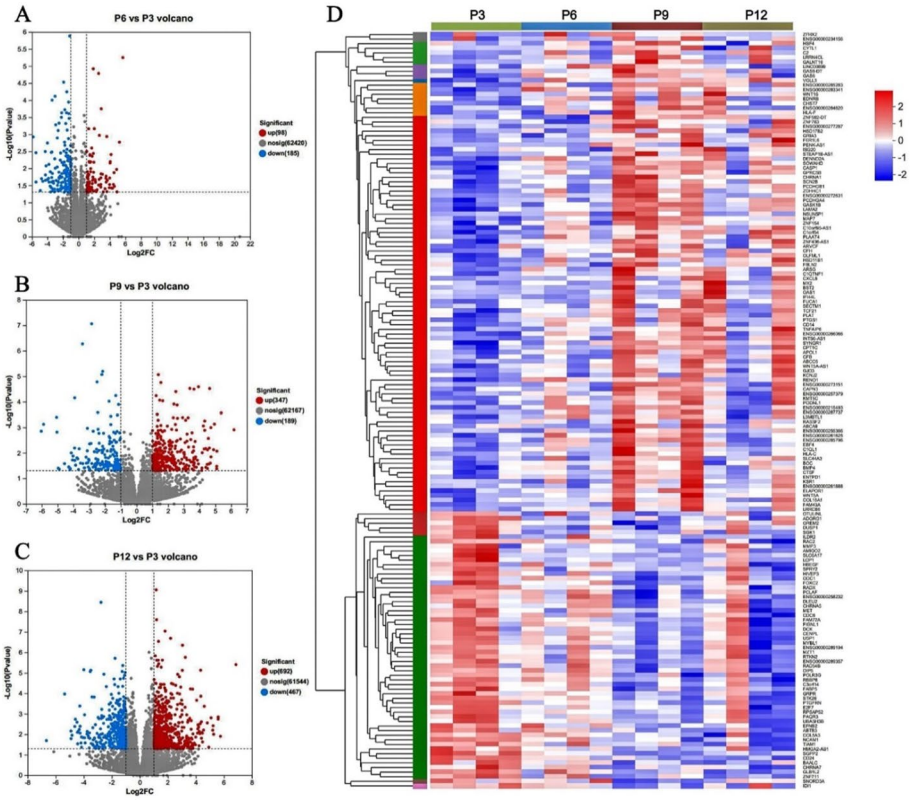

Fig. 4 Volcanograms and thermoclusters of DE mRNAs in DPSCs at P3, P6, P9, and P12. **A** P6 vs. P3 (volcanogram). **B** P9 vs. P3 (volcanogram). **C** P12 vs. P3 (volcanogram). **D** P3, P6, P9, and P12 (thermocluster)

Table 2 The mRNAs with the most significant fold changes between P12 and P3 (n = 4, mean ± SD)

Gene ID	Gene name	Log2FC[P12/P3]	Regulate
ENSG00000086696	HSD17B2	2.542375093	Up
ENSG00000002745	WNT16	1.808346941	Up
ENSG00000000971	CFH	1.438485741	Up
ENSG00000080573	COL5A3	− 1.055618779	Down
ENSG00000067064	IDI1	− 1.033491011	Down

pathways are shown in Fig. 5D. The top-ranked pathways included signalling pathways related to viral myocarditis, pertussis, coronavirus disease (COVID-19), and basal cell carcinoma, which are closely associated with human diseases.

PPI and co-expression network analysis

Compared with P3, a total of 70 nodes and 85 interaction pairs were identified in the PPI network in P12 DPSCs (Fig. 6). Nodes with high topological scores may play essential roles in DPSC aging in vitro. In this study, bone morphogenetic protein 4 (BMP4), interferon-stimulated exonuclease gene 20 (ISG20), type II transmembrane glycoprotein (BST2), and other DE mRNAs, such as Wnt family member 5A (WNT5A), were identified as essential genes in this network.

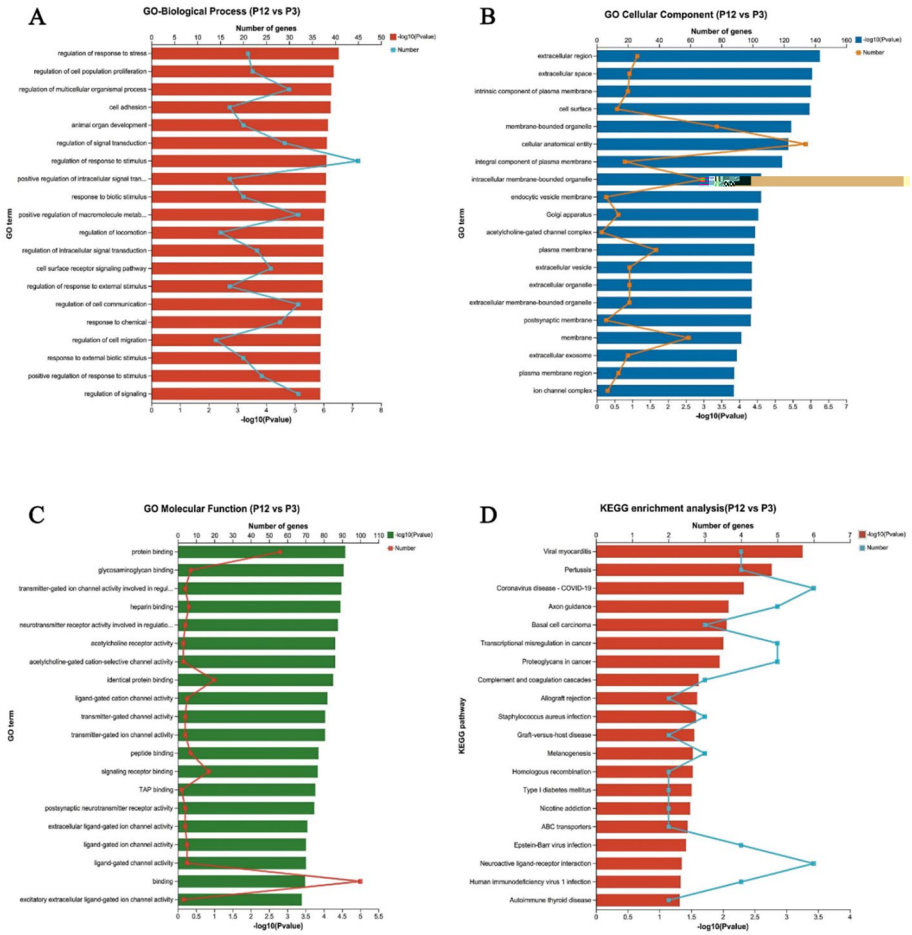

Fig. 5 GO and KEGG analysis of DE mRNAs between P12 and P3. **A**–**C** Top 20 items in biological processes, cellular components, and cellular functions, respectively. **D** Top 20 pathways

Validation of vital mRNAs expression

To verify the RNA-seq data and significant findings from the computational analysis, we performed quantitative real-time PCR for some critical mRNAs selected from the PPI networks. The expression levels of these mRNAs were measured in 4 human DPSCs at various passages. The qRT-PCR results showed that the expression of WNT16, CFH, and HSD17B2 was up-regulated, and that the expression of COL5A3 and IDI1 was down-regulated (Fig. 7). All qPCR results were consistent with the RNA-seq results, confirming the reliability of the sequencing results.

Discussion

DPSCs exhibit multidirectional differentiation potential, self-renewal, replication, and immunomodulation, and have promising applications in tissue engineering and cell therapy [16]. DPSCs, as a type of MSC, have a higher proliferation rate, greater in vivo osteoinductive formation and multidirectional differentiation potential compared to bone marrow MSCs [17]. Furthermore, DPSCs can be obtained from wisdom teeth or teeth that require extraction for orthodontic purposes, which is a straightforward process with

Table 3 GO analysis of top 10 terms with the most significant differences in biological processes

Term	Count	Rich ratio	*P* value	Candidate gene
Regulation of response to stress	21	0.143836	2.99E−07	FIGNL1; MET; EDNRB; CXCL6; USP1; RADX; POLR3G; UBAS-H3B; C1QTNF1; DUSP1; HBEGF; STK26; FOXC2; CFH; TNFAIP-6; RASSF2; HLAF; GPRC5B; WNT16; MMP3
Regulation of cell population proliferation	22	0.150685	4.53E−07	EFNB2; EDNRB; PLAAT4; ODC1; DUSP1; SGK1; GRPR; ADGR-G1; SPRY2; CD24; TIAM1; SGPP2; CHRNA7; BST2; HBEGF; PTG-S1; RAC2; RTKN2; COL18A1; E2F7; CDC6; HSF4
Regulation of multicellular organismal process	30	0.205479	5.46E−07	EFNB2; SCN2B; PLAAT4; ZFHX2; C1QTNF1; NSUN5P1; EDNR-B; POLR3G; SGK1; HLAF; L3MBTL1; TIAM1; CAPN3; UBASH3-B; SPRY2; CD24; CASP1; LAMA2; CD14; FABP5; KCNJ2; CHRN-A7; BST2; HBEGF; AMIGO2; RASSF2; GPRC5B; FOXC2; MET; C-XCL6
Cell adhesion	17	0.116438	5.72E−07	BOC; EFNB2; TNFAIP6; PCDHGB1; TIAM1; COL5A3; ENTPD1; ADGRG1; UBASH3B; COL18A1; ARVCF; NCAM1; CD24; PCDHGA4; RAC2; AMIGO2; LAMA2
Animal organ development	20	0.136986	7.04E−07	RTKN2; TCF21; CAPN3; MET; HSD17B2; ADGRG1; SLC6A17; ODC1; HSD11B1; HBEGF; COL5A3; GAS6; L3MBTL1; E2F7; AMI-GO2; LCP1; FOXC2; LAMA2; HSF4; ILDR2
Regulation of signal transduction	29	0.198630	7.70E−07	C1QTNF1; GREM2; L3MBTL1; TIAM1; ADGRG1; PAQR3; CAP-N3; UBASH3B; SPRY2; CD24; CASP1; CD14; FABP5; CHRNA7; BST2; DUSP1; HBEGF; GRIA3; RAC2; RASSF2; GPRC5B; RTKN-2; TCF21; FIGNL1; MET; SECTM1; NCAM1; RBBP8; WNT16
Regulation of response to stimulus	45	0.308219	8.04E−07	EFNB2; TNFAIP6; TIAM1; C1QTNF1; GREM2; EDNRB; POLR3-G; HLAF; L3MBTL1; FABP5; ADGRG1; PAQR3; CAPN3; UBAS-H3B; SPRY2; CXCL6; CD24; CASP1; STK26; NCAM1; CFB; CD14; C2; CHRNA7; CFH; RADX; BST2; DUSP1; HBEGF; MMP3; GRI-A3; RAC2; RASSF2; GPRC5B; FOXC2; RTKN2; TCF21; FIGNL1; MET; SECTM1; RBBP8; USP1; HLAC; WNT16
Positive regulation of intracellular signal transduction	17	0.116438	8.39E−07	RTKN2; MET; CD14; TIAM1; ADGRG1; SECTM1; C1QTNF1; BST2; HBEGF; SPRY2; CD24; RAC2; CASP1; RASSF2; CHRNA7; G-PRC5B; WNT16
Response to biotic stimulus	20	0.136986	8.47E−07	APOL1; GRPR; EDNRB; POLR3G; CD14; C2; CXCL6; ISG20; OD-C1; CFB; BST2; IFI44L; CASP1; MX2; CD24; FER1L6; CFH; OAS1-; HLAC
Positive regulation of macromolecule metabolic process	32	0.219178	9.67E−07	EDNRB; C1QTNF1; NSUN5P1; CYTL1; POLR3G; HLAF; MYBL1; ZFHX2; CAPN3; SPRY2; EBF4; CD24; CASP1; STK26; CD14; TIAM1; ZNF711; WNT5A; CHRNA7; HBEGF; RASSF2; GPRC5B; FOXC2; TCF21; MET; GAS6; HIVEP3; HSF4; E2F7; CDC6; WNT16

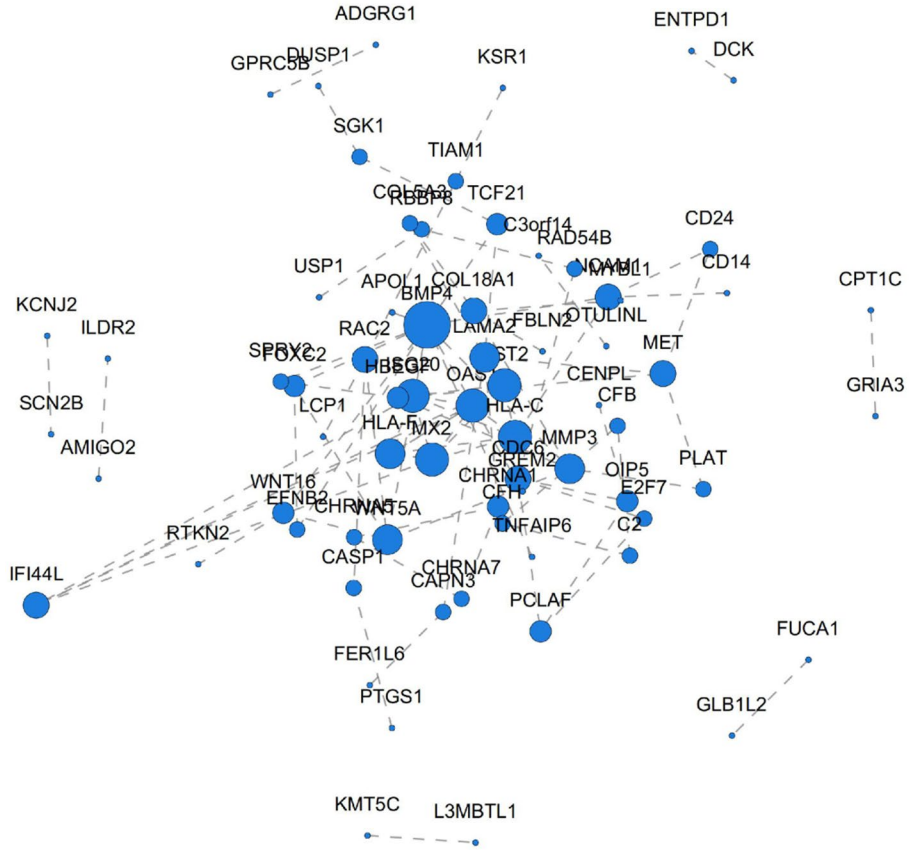

Fig. 6 Analysis of the protein interactions between P12 and P3. Nodes indicate genes, and edges indicate the interactions between two genes; the more edges connected to one node, the greater its degree, and the larger the node, the more significant the importance of the gene in this network

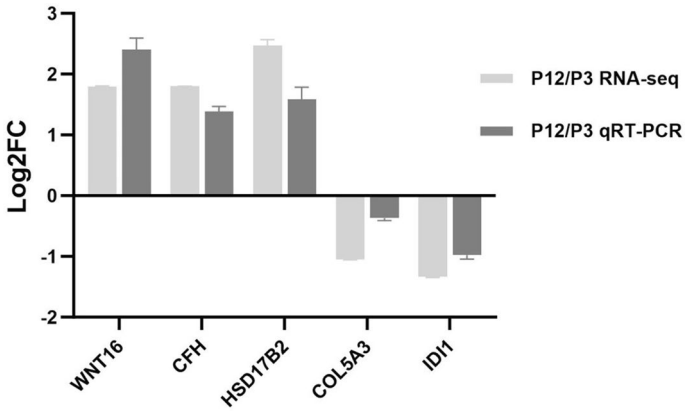

Fig. 7 Changes in the expression of 5 critical mRNAs between P12 and P3 were analysed by RNA-seq and qRT-PCR (n = 4)

less trauma to patients and involves fewer ethical considerations [18]. A study by Pilbauerova et al. [19] demonstrated that following thawing after cryopreservation for 1 year at −80 °C, the cell viability, proliferative capacity, and differentiation ability of DPSCs

remained unaffected. These advantages have expanded the clinical applications of DPSCs. Studies have demonstrated that DPSCs must be expanded and cultured in vitro to meet clinical treatment needs [3]. Nevertheless, prolonged in vitro expansion and culture result in cellular senescence. Current research on cellular senescence resulting from prolonged in vitro expansion and culture has primarily focused on other types of stem cells, with few studies focusing on DPSC senescence. Further research is required to elucidate the related aspects of DPSCs and the mechanisms underlying senescence. This will facilitate the determination of the optimal number of in vitro expansion generations to ensure that the cell activity and number meet clinical therapeutic application requirements [3].

In this study, we successfully established a DPSC senescence model by extracting primary DPSCs and culturing them for 12 generations via in vitro expansion under standard culture conditions. DPSCs cultured to the third generation were selected as the control population, flow cytometry was performed to detect the expression of antigenic markers on their surfaces, and osteogenic–lipogenic induction was performed. The results demonstrated that the negative markers CD34 and CD45 were expressed at low levels, whereas the positive markers CD73, CD90, and CD105 were highly expressed. Furthermore, the flow cytometry results were consistent with the surface immunostaining profiles of MSCs, as previously reported [20]. These findings indicated that the extracted cells exhibited the potential for osteoblastic and lipogenic differentiation, which confirmed that the cells were MSCs. Following a prolonged period of in vitro passaging and expansion culture, it was observed that the proliferative capacity of the cells declined, accompanied by a gradual increase in the proportion of SA-β-gal-positive cells with each additional passage. SA-β-gal is a marker of cellular senescence, suggesting that DPSCs exhibit a gradual process of cellular senescence with an increase in the number of passages [21]. Although DPSCs continued to exhibit low expression levels of CD34 and CD45, there was a tendency for CD73, CD90, and CD105 expression to decline with the number of passages, with the most significant decrease observed after in vitro expansion to 12 generations. The results of the osteogenic–lipogenic induction experiments demonstrated that the differentiation potential of DPSCs was reduced with an increase in the number of in vitro amplifications. These experimental results are consistent with those of previous studies [22, 23]. The experimental results suggest that DPSCs with reduced polydifferentiation potential after aging may no longer be suitable for clinical treatment.

However, there is a divergence of opinions regarding the changes in stem cell surface markers with passaging. Kim et al. [24] studied 55 generations of bone marrow MSCs cultured in vitro and found that the expression of stem cell surface markers tended to stabilise with an increasing number of passages. In contrast, some researchers expanded DPSCs in vitro for up to 12 generations and found that the expression of STRO-1, a surface marker of DPSCs, decreased with an increasing number of passages, while the expression of CD73, CD90 and CD105 remained relatively stable [25, 26]. This was not consistent with our experimental results. The experimental results may have been affected by various factors, including the source of the pulp tissue, stage of tooth development, and age of the patient. In addition, heterogeneity may increase during the culture process owing to differences in culture time, medium used, and number of passages. There are few studies on the expression of surface markers in DPSCs with different

numbers of passages, which requires further exploration. There are currently no specific surface markers for DPSCs [26, 27]. The typical markers for MSCs, including CD73, CD90, and CD105, do not appear to provide sufficient or specific indications to maintain the 'stemness' of DPSCs. Therefore, additional stem cell markers and other multiparametric immunophenotyping methods should be employed to validate the stemness of DPSCs.

The mRNA expression profiles reflect the biological behaviour and function of DPSCs cultured in vitro for long periods. Changes in mRNA expression profiles are closely associated with functional changes during aging in vitro. This experimental study identified a series of mRNAs associated with DPSC senescence and their associated molecular mechanisms, which may be potential mediators of changes in biological properties, such as reduced proliferation and differentiation, after long-term in vitro expansion and culture. A total of 1159 DE mRNAs were identified between P12 and P3. Further analysis of these DE mRNAs revealed that changes in CFH, WNT16, IDI1, COL5A3, and HSD17B2 mRNA levels were closely associated with cellular senescence. CFH is a complement inhibitor that plays a crucial role in complement homeostasis [28]. The sequencing results demonstrated that CFH exhibited elevated expression in senescent DPSCs subjected to long-term expansion and in vitro culture. Furthermore, mutations and variants of CFH are significantly associated with several human age-related diseases, including cancer and age-related macular degeneration [28–30]. Wnt16, a member of the Wnt family, has been shown to be closely associated with osteogenic differentiation, cellular senescence, and tumourigenesis [31–33]. Additionally, it has been implicated in stem cell proliferation and differentiation [34]. The RNA-seq results demonstrated that WNT16 gene expression was up-regulated, whereas the osteogenic induction assay results indicated that the osteogenic capacity of stem cells gradually declined with increasing passages. This suggests that elevated WNT16 expression inhibits osteogenic differentiation. Jiang et al. [35] demonstrated that the Wnt/β-catenin protein signalling pathway inhibits the osteogenic differentiation of human MSCs and MC3T3-E1 cells (mouse embryonic osteoblasts) [35–37]. This is consistent with the findings of our experiments. However, Meyers et al. [38] proposed that WNT16 stimulates the osteogenic differentiation of perivascular stem cells (PSC). These disparate findings indicate that the Wnt signalling pathway plays a pivotal role in the regulatory network of endosteal homeostasis. Overactivation and inactivation of Wnt signalling can result in skeletal deformities, bone diseases, and cartilage loss [39]. The number of studies investigating WNT16 and osteogenic differentiation of stem cells is limited, and the role of this gene in the osteogenesis of DPSCs remains to be elucidated. IDI1 encodes a peroxisomal-localisation enzyme that removes toxic hydrogen peroxide produced by different oxidative enzymes in the peroxisomal respiratory pathway [40]. It is involved in processes such as cell division and proliferation, and is associated with age-related diseases [41]. The experimental results demonstrated that the expression of IDI1 was reduced in senescent DPSCs. This reduction in the synthesis of peroxisome-localised enzymes and the catabolism of hydrogen peroxide exacerbates cellular senescence. Collagen type V alpha 3 chain (COL5A3) is a member of the collagen family that is closely associated with osteogenesis and tumourigenesis. The results indicated that cellular senescence was associated

with a reduction in COL5A3 expression. Jadaun et al. [42] demonstrated that hypoxia stimulates the expression of COL1A1, COL5A1, and COL5A3 in osteoblasts, which play a role in maintaining bone volume by promoting collagen production. Chen et al. [43] observed that collagen inhibits immune signalling in the tumour microenvironment (chemokine production), thereby inhibiting antitumour immune responses. The loss of collagen results in an increase in chemokine levels, which in turn facilitates the proliferation of cancer cells. 17-β-Hydroxysteroid dehydrogenase type 2 (HSD17B2) is associated with oestrogen synthesis and regulates oestradiol (E2) [44]. The results indicated that HSD17B2 expression was up-regulated, suggesting that it may be associated with cellular senescence. Lu et al. [44] demonstrated that the inhibition of HSD17B2 activity suppresses E2 inactivation, increases endogenous oestrogen levels, and improves bone metabolism-related indicators. In conclusion, these changes in DE mRNA are closely associated with cellular senescence, disease development, and osteogenic differentiation. One limitation of this study is that we did not perform a gene knockdown. Further studies are required to determine the effects of gene knockdown on DPSC senescence.

KEGG analysis identified numerous signalling pathways associated with human diseases, including viral myocarditis, pertussis, COVID-19, and basal cell carcinoma. These pathways play a pivotal role in the functional changes induced by aging, thereby underscoring the significance of DPSC aging in the pathogenesis and clinical treatment of cancer and metabolic diseases.

Among the interactions between DE-encoded proteins, BMP4, ISG20, BST2, and Wnt5a were identified as key genes interacting with many other DE mRNAs in this network. BMP4, a member of the TGF-β superfamily, is involved in a variety of biologically regulated processes such as cell proliferation and cellular differentiation [45]. BMP4 plays a key role in bone formation and may promote alveolar bone development by increasing the expression of Runx2, BSP, and OCN [46]. ISG20 has been associated with certain RNA virus-induced diseases, and a study on the antiviral mechanisms of ISG20 showed that the overexpression of recombinant ISG20 in cultured cells increased cellular resistance to infection with certain viral RNA genomes [47, 48]. BST2, also known as CD317, is involved in a variety of physiological and pathological processes, including inflammation, immune regulation, and tumourigenesis, and is overexpressed in various malignant tumours, suggesting that it may be associated with certain tumour disorders induced by cellular senescence [34, 49–51]. Wnt5a, a representative Wnt protein of the non-classical Wnt signalling pathway, plays an important role in the development and maturation of various tissues and organs and is closely related to a variety of diseases, such as infectious diseases, cancer, and metabolic disorders [52]. Studies on Wnt5a and related aspects of its signalling pathway may provide new ideas for the diagnosis and treatment of human diseases [53]. In summary, these proteins are closely related to the biological changes in DPSCs after long-term in vitro amplification and culturing. However, the use of these proteins as clinical detection markers requires further investigation.

DPSCs are derived from neural crest cells and have unique advantages in nerve repair, cartilage formation, and corneal reconstruction [54–57]. Furthermore, in addition to its use in repairing teeth and maxillofacial bone tissue, DPSCs can be used to

repair tissues outside the oral cavity, such as nerves and cartilage. DPSCs are receiving increasing attention in regenerative medicine; autologous stem cell therapy is promising for diabetes and myocardial infarction [58, 59].

DPSCs extracted using the pulp tissue block method exhibited low CD34 and CD45 expression and high CD73, CD90, and CD105 expression, and demonstrated osteogenic and lipogenic differentiation potential. The number of in vitro expansions was found to induce cellular senescence of pulp stem cells, resulting in a reduction in the proliferative capacity and osteogenic and lipogenic differentiation potentials. Changes in mRNA expression induced by prolonged expansion in vitro may be a potential mechanism for the senescence of DPSCs. The differential expression of genes, including CFH, WNT16, HSD17B2, IDI, and COL5A3, may be important in the context of pulp stem cell senescence, and it is crucial to explore the molecular mechanism underlying the senescence of DPSCs to establish a more robust theoretical basis for clinical applications.

Materials and methods

Cell isolation and passaging

This study was approved by the Ethics Committee of Qingdao Stomatological Hospital, Qingdao University (2022KQYX023; 1 October 2023–1 May 2024). Twenty orthodontic patients (10 males and 10 females) aged 12 to 16 without systemic diseases were enrolled in this study. Teeth without dental or periodontal disease were isolated from these patients within 1 week, and pulp tissues were isolated from the teeth within 4 h using the tissue block method. Pulp tissue from each tooth was cultured separately as independent samples to isolate DPSCs. The cells were passaged at 80% cell density and grown in vitro for up to 12 generations. This study analysed DPSCs from the third, sixth, ninth, and twelfth generations. The DPSCs were cultured in α-MEM medium (Pricella, Wuhan, China) with varying concentrations of foetal bovine serum (Pricella) and 1% penicillin–streptomycin (BioIndustries, Israel) according to the specific experimental conditions. All cells were maintained at 37 °C under a constant humidity of 5% CO_2.

Flow cytometry

Flow cytometry was used to assess the presence of positive (CD73, CD90, and CD105) and negative (CD34 and CD45) markers in DPSCs. Cells at P3, P6, P9, and P12 were digested and centrifuged. The cell density was subsequently standardised to 1×10^4 cells/mL, and 100 μL cell suspension was added to the centrifuge tube. Anti-human antibodies for CD34 (E-AB-F1143C), CD45 (E-AB-F1137C), CD73 (E-AB-F1242D), CD90 (E-AB-F1167D), and CD105 (E-AB-F1143D) (Elabscience, Wuhan, China) were added in a ratio of 50:1. Phosphate-buffered saline (PBS; Pricella) served as a control. The supernatant was centrifuged and discarded after an incubation for 1 h in the dark at room temperature, followed by two washes with PBS and resuspension in 500 μL PBS. The expression levels of various antibodies were determined by flow cytometry using a DxFLEX machine (Beckman Coulter, Suzhou, China).

Cell proliferation

Cell Counting Kit-8 (CCK-8; Beyotime, Shanghai, China) was used to measure cell proliferation according to the manufacturer's instructions. DPSCs at P3, P6, P9, and P12

were seeded at a density of 1×10^4 cells/well in 96-well culture plates and incubated for 1–5 d. At each specific time point, the complete medium was exchanged with new α-MEM basal medium supplemented with a 10% CCK-8 solution. The solution was incubated in the dark for 2 h at 37 °C. Finally, the cell proliferation capacity was determined by measuring the absorbance at 450 nm using an enzyme label reader (SynergyH1/H1M, Bio-Tek, Beijing, China).

Cellular senescence

Cellular senescence was detected through β-galactosidase staining. DPSCs at P3, P6, P9, and P12 were introduced in 6-well plates at a density of 1×10^5 cells/well. The SA-β-gal activity was then evaluated using the β-galactosidase staining kit (Beyotime) according to the manufacturer's instructions. Senescent cells were stained blue by SA-β-gal, and SA-β-gal positive cells were evaluated as a percentage of all cells based on three randomly selected fields.

Osteogenic differentiation

DPSCs at P3, P6, P9, and P12 were plated in 6-well dishes at a density of 2×10^5 cells/well until they reached 70% confluence. The original medium was aspirated and replaced with osteogenic differentiation-inducing medium (Pricella). The cells were cultured for 21 d and the medium was changed every 3 d. After fixation with 4% paraformaldehyde, the samples were stained with ARS and washed with PBS. Images were obtained using an optical microscope (OLYMPUS, Tokyo, Japan). Then, a 10% Cetylpyridinium Chloride solution was added to the wells, and the solution was dissolved for 30 min at room temperature. The decolourised solution was collected, and the absorbance at 562 nm was measured using an enzyme label reader.

Lipogenic differentiation

DPSCs at P3, P6, P9, and P12 were seeded in 6-well plates at 2×10^5 cells/well. After the cells reached 100% confluence, the original medium was removed and lipid induction was carried out for 14 d using a lipid-forming differentiation-inducing medium (Pricella) following the manufacturer's instructions. The cells were fixed using 4% paraformaldehyde solution (Elabscience), washed with PBS, and stained with ORO. Following observation and capture of images under a light microscope, the stained lipid droplets were dissolved in isopropanol (Sigma-Aldrich) at room temperature, the decolourised solution was collected, and the absorbance at 520 nm was measured using an enzyme label reader.

Library construction and high-throughput sequencing

RNA extraction

Total RNA was extracted from P3, P6, P9, and P12 stem cells ($n = 4$) using the TRIzol reagent (Pricella) according to the manufacturer's instructions. The RNA quality was determined using a 5300 Bioanalyzer (Agilent Technologies) and quantified using an ND-2000 spectrophotometre (NanoDrop Technologies). High-quality RNA samples (OD260/280 = 1.8–2.2, OD260/230 ≥ 2.0, RIN ≥ 6.5, 28S:18S ≥ 1.0, > 1 μg) were used to construct sequencing libraries.

Library preparation and sequencing

RNA purification, reverse transcription, library construction, and sequencing were performed at Shanghai Majorbio Bio-Pharm Biotechnology Co., Ltd., Shanghai, China, according to the manufacturer's instructions (Illumina, San Diego, CA, USA). The mRNA-seq transcriptome libraries were prepared with 1 μg of total RNA following the Illumina® Stranded mRNA Prep, Ligation method. mRNA was isolated by poly (A) selection using oligo (dT) beads, followed by fragmentation with fragmentation buffer. Double-stranded cDNA was synthesised using a SuperScript double-stranded cDNA synthesis kit (Invitrogen, Carlsbad, CA, USA) and random hexamer primers (Illumina). According to Illumina's library construction protocol, the synthesised cDNAs were subjected to end repair, phosphorylation, and 'A' base addition. The 300 bp cDNA target fragment was size-screened on 2% Low Range Ultra Agarose, followed by 15 cycles of PCR amplification using Phusion DNA polymerase (NEB). After quantification using Qubit 4.0, paired-end RNA-seq libraries were sequenced using a NovaSeq 6000 sequencer (2×150 bp read length).

Quality control and read mapping

Raw paired-end reads were trimmed and quality-controlled using fast and default parameters. Clean reads were individually aligned to the reference genome in targeted mode using the HISAT2 software. Mapped reads for each sample were assembled on a reference basis using the StringTie software.

Differential expression analysis and functional enrichment

To identify differentially expressed genes (DEGs) between the two samples, the expression level of each transcript was calculated based on the transcripts per million reads (TPM) method. RSEM was used to quantify the gene abundance. Differential expression analyses were performed using DESeq2 and DEGseq. DEGs with $|\log2FC| \geq 1$ and FDR < 0.05 (DESeq2) or FDR < 0.001 (DEGseq) were considered significant DEGs. Functional enrichment analyses, including GO and KEGG, were also performed, and DEGs were found to be significantly enriched in GO terms and metabolic pathways (Bonferroni-corrected *P*-value < 0.05). GO functional enrichment and KEGG pathway analysis were performed using Goatools and SciPy, respectively.

Quantitative real-time PCR

Total RNA was extracted from all groups, and the RNA concentration was assessed using a Micro Drop ultra-microspectrophotometer (Bio DL, Texas, USA). All samples used GAPDH (Abcam, Cambridge, UK) as an internal reference, and the mRNA expression levels of WNT16 (Sangon Biotech, Shanghai, China), CFH (Sangon Biotech), COL5A3 (Sangon Biotech), HSD17B2 (Sangon Biotech) and IDI (Sangon Biotech) were quantified using the $2^{-\Delta\Delta CT}$ method. The primers used were WNT16: 22 ATC GGA AAC ACC ACG GGC AAA G (forward) and 24 CAG CGG CAG TCT ACT GAC ATC AAC (reverse); CFH: 132 GAA GGA TGT GTA TAA GGC GGG TGA G (forward) and 132 CAG GAG GTG TCT CTG CAT GTT GG (reverse); COL5A3: 19 ACC CGC ACC TGC CTG ATG G (forward) and 21 TCT CCT CCC

GCC GTG AAG TTG (reverse); HSD17B2: 22 AGT CTG CCT GCT CAT CCT GTC C (forward) and 21 CCG CAA TCA CCA CCT GTC ACC (reverse); IDI: 117 CCG CAT CCA CTA CGC AGA CAC (forward) and 117 ACC TCA CTG ACC TCG TTG CTA TTT G (reverse).

Statistical analysis

The experiments were conducted thrice in each group, and the outcomes were represented as mean ± standard deviation. To compare various groups, we used one-way analysis of variance (ANOVA) and Tukey's post-hoc test (pairwise comparison). Data were statistically analysed using GraphPad Prism 10 software. Differences between groups were considered significant at $P < 0.05$.

Author contributions

A and F conceptualized the study. A and B designed the method. A and C performed data analysis. E and D provided resources and interpreted the data. A and E performed data acquisition. A wrote the original draft preparation, and F reviewed and edited the manuscript. F supervised the study. All authors have read and agreed to the published version of the manuscript.

Funding

This work was supported by Qingdao Chinese Medicine Science and Technology Project (2022-ZYYQ04), Qingdao Key Health Discipline Development Fund (2020–2022), and Qingdao Clinical Research Center for Oral Diseases (22-3-7-lczx-7-nsh).

Data availability

No datasets were generated or analysed during the current study.

Declarations

Ethics approval and consent to participate

The study was conducted in accordance with the Declaration of Helsinki and was approved by the Ethics Committee of Qingdao Stomatological Hospital (2022KQYX023, September 2022). Informed consent was obtained from all subjects involved in the study. Written informed consent has been obtained from the patient(s) to publish this paper.

Competing interests

The authors declare no competing interests.

Received: 23 July 2024 Accepted: 7 October 2024
Published online: 18 October 2024

References

1. Zhao R, et al. Bone grafts and substitutes in dentistry: a review of current trends and developments. Molecules. 2021;26(10):3007.
2. Al-Azab M, et al. Aging of mesenchymal stem cell: machinery, markers, and strategies of fighting. Cell Mol Biol Lett. 2022;27(1):69.
3. Morsczeck C. Cellular senescence in dental pulp stem cells. Arch Oral Biol. 2019;99:150–5.
4. Shen WC, et al. Methylation and PTEN activation in dental pulp mesenchymal stem cells promotes osteogenesis and reduces oncogenesis. Nat Commun. 2019;10(1):2226.
5. Ma L, et al. Maintained properties of aged dental pulp stem cells for superior periodontal tissue regeneration. Aging Dis. 2019;10(4):793–806.
6. Gronthos S, et al. Postnatal human dental pulp stem cells (DPSCs) in vitro and in vivo. Proc Natl Acad Sci USA. 2000;97(25):13625–30.
7. Alongi DJ, et al. Stem/progenitor cells from inflamed human dental pulp retain tissue regeneration potential. Regen Med. 2010;5(4):617–31.
8. Sun HH, et al. Investigation of dental pulp stem cells isolated from discarded human teeth extracted due to aggressive periodontitis. Biomaterials. 2014;35(35):9459–72.
9. Tatullo M, et al. Dental pulp stem cells: function, isolation and applications in regenerative medicine. J Tissue Eng Regen Med. 2015;9(11):1205–16.
10. Dong XY, et al. Downregulation of ROR2 promotes dental pulp stem cell senescence by inhibiting STK4-FOXO1/SMS1 axis in sphingomyelin biosynthesis. Aging Cell. 2021;20(8): e13430.
11. Estrada JC, et al. Human mesenchymal stem cell-replicative senescence and oxidative stress are closely linked to aneuploidy. Cell Death Dis. 2013;4(6): e691.

12. Morsczeck C, et al. The cell cycle regulator protein P16 and the cellular senescence of dental follicle cells. Mol Cell Biochem. 2018;439(1–2):45–52.
13. Casella G, et al. mRNA methylation in cell senescence. Wiley Interdiscip Rev RNA. 2019;10(6): e1547.
14. Batista PJ. The RNA modification N(6)-methyladenosine and its implications in human disease. Genom Proteom Bioinform. 2017;15(3):154–63.
15. Cao G, et al. Recent advances in dynamic m6A RNA modification. Open Biol. 2016;6(4): 160003.
16. Yoshida S, et al. Insight into the role of dental pulp stem cells in regenerative therapy. Biology. 2020;9(7):160.
17. Feng X, et al. TNF-alpha triggers osteogenic differentiation of human dental pulp stem cells via the NF-kappaB signalling pathway. Cell Biol Int. 2013;37(12):1267–75.
18. Munsie M, Hyun I. A question of ethics: selling autologous stem cell therapies flaunts professional standards. Stem Cell Res. 2014;13(3 Pt B):647–53.
19. Pilbauerova N, et al. The effects of cryogenic storage on human dental pulp stem cells. Int J Mol Sci. 2021;22(9):4432.
20. Dominici M, et al. Minimal criteria for defining multipotent mesenchymal stromal cells. The international society for cellular therapy position statement. Cytotherapy. 2006;8(4):315–7.
21. Stenderup K, et al. Aging is associated with decreased maximal life span and accelerated senescence of bone marrow stromal cells. Bone. 2003;33(6):919–26.
22. de Farias JO, Rezende T. Dental pulp and apical papilla cells senescence: causes, consequences, and prevention. Biogerontology. 2023;24(4):533–9.
23. He X, et al. ROR2 downregulation activates the MSX2/NSUN2/p21 regulatory axis and promotes dental pulp stem cell senescence. Stem Cells. 2022;40(3):290–302.
24. Kim J, et al. Biological characterization of long-term cultured human mesenchymal stem cells. Arch Pharm Res. 2009;32(1):117–26.
25. Gao L, et al. Exploring the stem cell surface markers expressed in human dental pulp stem cells. Shanghai Kou Qiang Yi Xue. 2015;24(3):257–62.
26. Ducret M, et al. Phenotypic identification of dental pulp mesenchymal stem/stromal cells subpopulations with multiparametric flow cytometry. Methods Mol Biol. 2019;1922:77–90.
27. Liang JF, et al. Identification of dental stem cells similar to skeletal stem cells. J Dent Res. 2022;101(9):1092–100.
28. Boon CJ, et al. The spectrum of phenotypes caused by variants in the CFH gene. Mol Immunol. 2009;46(8–9):1573–94.
29. Yoon YH, et al. Upregulation of complement factor H by SOCS-1/3–STAT4 in lung cancer. Cancers. 2019;11(4):471.
30. Deng Y, et al. Age-related macular degeneration: epidemiology, genetics, pathophysiology, diagnosis, and targeted therapy. Genes Dis. 2022;9(1):62–79.
31. Garcia-Ibarbia C, et al. Missense polymorphisms of the WNT16 gene are associated with bone mass, hip geometry and fractures. Osteoporos Int. 2013;24(9):2449–54.
32. Binet R, et al. WNT16B is a new marker of cellular senescence that regulates p53 activity and the phosphoinositide 3-kinase/AKT pathway. Cancer Res. 2009;69(24):9183–91.
33. Nusse R. Wnt signaling in disease and in development. Cell Res. 2005;15(1):28–32.
34. Nusse R, Clevers H. Wnt/beta-catenin signaling, disease, and emerging therapeutic modalities. Cell. 2017;169(6):985–99.
35. Jiang Z, et al. Wnt16 is involved in intramembranous ossification and suppresses osteoblast differentiation through the Wnt/beta-catenin pathway. J Cell Physiol. 2014;229(3):384–92.
36. de Boer J, et al. Wnt signaling inhibits osteogenic differentiation of human mesenchymal stem cells. Bone. 2004;34(5):818–26.
37. Kahler RA, Westendorf JJ. Lymphoid enhancer factor-1 and beta-catenin inhibit Runx2-dependent transcriptional activation of the osteocalcin promoter. J Biol Chem. 2003;278(14):11937–44.
38. Meyers CA, et al. WNT16 induces proliferation and osteogenic differentiation of human perivascular stem cells. J Orthop. 2018;15(3):854–7.
39. Ye X, Liu X. Wnt16 signaling in bone homeostasis and osteoarthritis. Front Endocrinol. 2022;13:1095711.
40. Fransen M, et al. Aging, age-related diseases and peroxisomes. Subcell Biochem. 2013;69:45–65.
41. Fransen M, et al. Role of peroxisomes in ROS/RNS-metabolism: implications for human disease. Biochim Biophys Acta. 2012;1822(9):1363–73.
42. Jadaun PK, et al. Inhibition of hypoxia-induced Mucin 1 alters the proteomic composition of human osteoblast-produced extracellular matrix, leading to reduced osteogenic and angiogenic potential. J Cell Physiol. 2022;237(2):1440–54.
43. Chen Y, et al. Type I collagen deletion in alphaSMA^{+} myofibroblasts augments immune suppression and accelerates progression of pancreatic cancer. Cancer Cell. 2021;39(4):548-565.e6.
44. Lu Y, et al. Psoralen prevents the inactivation of estradiol and treats osteoporosis via covalently targeting HSD17B2. J Ethnopharmacol. 2023;311: 116426.
45. Pan Y, et al. Role and mechanism of BMP4 in regenerative medicine and tissue engineering. Ann Biomed Eng. 2023;51(7):1374–89.
46. Ou M, et al. Bmp2 and Bmp4 accelerate alveolar bone development. Connect Tissue Res. 2015;56(3):204–11.
47. Espert L, et al. ISG20, a new interferon-induced RNase specific for single-stranded RNA, defines an alternative antiviral pathway against RNA genomic viruses. J Biol Chem. 2003;278(18):16151–8.
48. Horio T, et al. Crystal structure of human ISG20, an interferon-induced antiviral ribonuclease. FEBS Lett. 2004;577(1–2):111–6.
49. Tiwari R, et al. Beyond tethering the viral particles: immunomodulatory functions of tetherin (BST-2). DNA Cell Biol. 2019;38(11):1170–7.
50. Mahauad-Fernandez WD, Okeoma CM. The role of BST-2/tetherin in host protection and disease manifestation. Immun Inflamm Dis. 2016;4(1):4–23.
51. Swiecki M, Omattage NS, Brett TJ. BST-2/tetherin: structural biology, viral antagonism, and immunobiology of a potent host antiviral factor. Mol Immunol. 2013;54(2):132–9.

52. Cheng CW, et al. Wnt5a-mediated non-canonical Wnt signalling regulates human endothelial cell proliferation and migration. Biochem Biophys Res Commun. 2008;365(2):285–90.
53. Kikuchi A, et al. Wnt5a: its signalling, functions and implication in diseases. Acta Physiol. 2012;204(1):17–33.
54. Lumsden AG. Spatial organization of the epithelium and the role of neural crest cells in the initiation of the mammalian tooth germ. Development. 1988;103(Suppl):155–69.
55. Luke AM, et al. Human dental pulp stem cells differentiation to neural cells, osteocytes and adipocytes—an in vitro study. Heliyon. 2020;6(1): e03054.
56. Longoni A, et al. The chondrogenic differentiation potential of dental pulp stem cells. Eur Cell Mater. 2020;39:121–35.
57. Mead B, et al. Concise review: dental pulp stem cells: a novel cell therapy for retinal and central nervous system repair. Stem Cells. 2017;35(1):61–7.
58. Govindasamy V, et al. Differentiation of dental pulp stem cells into islet-like aggregates. J Dent Res. 2011;90(5):646–52.
59. Gandia C, et al. Human dental pulp stem cells improve left ventricular function, induce angiogenesis, and reduce infarct size in rats with acute myocardial infarction. Stem Cells. 2008;26(3):638–45.

Publisher's Note